RSC Advances

ROYAL SOCIETY OF CHEMISTRY

www.rsc.org/advances

RSC Advances

ARTICLE

Core/shell structured covalently bonded TiO_2/poly(3,4-ethylenedioxythiophene) dispersions and their electrorheological responses: Effect of anisotropy

Received 00th January 20xx,
Accepted 00th January 20xx

DOI: 10.1039/x0xx00000x

www.rsc.org/

O. Erol,[a,b] and H. I. Unal*[,a]

As a new electrorheological (ER) material, core/shell nanorod consists of a titania core and conducting polymer poly(3,4-ethylenedioxythiophene) (PEDOT) shell was prepared via covalent bonding to achieve thin polymer shell and make interfacial interactions between the two components more impressive. The successful coating of PEDOT on the nanorod-TiO_2 particles was proved by TEM analysis. The antisedimentation stability of the core/shell nanorod-TiO_2/PEDOT particles were determined to be 100%. ER properties of the materials were studied under controlled shear, oscillatory shear and creep tests. The dielectric spectra of the dispersions were recorded to further understand their ER responses and fitted with the Cole–Cole equation. The ER behavior of the dispersions was also observed by an optical microscope. The flow curves of these ER fluids were determined under various electric field strengths and their flow characteristics were examined via rheological equation of Cho–Choi–Jhon (CCJ) model. Further, the results were also compared with nanoparticle-TiO_2/PEDOT. It was concluded that conducting thin polymer shell and elongated structure of the hybrid material made synergistic effect on electric field induced polarizability and colloidal stability against sedimentation and resulted in with the stronger ER activity, storage modulus and higher recovery after stress loadings compared to nanoparticle-TiO_2/PEDOT.

Introduction

Electrorheological (ER) fluids are classified as smart materials that consist of polarizable particles in an insulating liquid such as silicon oil (SO). ER fluids change their microstructural and rheological properties reversibly and rapidly from randomly distributed liquid state to solid-like state under externally applied electric fields by forming chain or columnar-like structures along the direction of the fields.[1] This reversible transition enables the ER fluids to find potential applications in many devices such as clutches,[2] shock absorbers,[3] dampers,[4] human muscle stimulators,[5] polishing,[6] microfluidic chip and pumps,[7] and etc. However, higher yield stress, durability in wide temperature range, stability of dispersions against gravitational forces and lower zero-field viscosity are required for practical applications and many efforts have been exerted to improve the performance of the ER fluids.[8] It is well known that the geometry of the dispersed particles affects the dielectric properties of the dispersions which is closely correlated with polarizability and ER effect under applied electric field. Especially, elongated particles rather than spherical ones is expected to show higher electric field induced dipole moments which lead stronger polarization and enhanced ER effect as well as higher colloidal stability of dispersion.[9,10] Therefore, many one-dimensional materials such as polyaniline nanofiber,[11] goethite nanorod,[9] rod-like titania,[12] rod-like calcium titanyl oxalate,[13] silica coated MWCNT[14] have been reported as the ER active materials.

Researchers have made many efforts to explore various promising materials based on ER fluids which include consideration of inorganic and polymeric materials such as metal oxides,[15,16] porous particles[17,18] conducting polymers and their composites,[19,20] carbonaceous particles,[21] and core–shell nanoparticles.[14,22] Among these materials, titania is frequently studied as a potential ER active material because of its stability against high electric field strengths and suitable dielectric constant.[23,24] To synthesize titania having various morphologies including elongated structures such as nanotubes, nanowires and nanofibers is also possible. One-dimensional anisotropic titania nanostructures especially become interesting by combining high aspect ratio and specific surface area. But, similar to the other inorganic nanoparticles, titania tends to agglomerate in insulating liquid because of its highly hydrophilic character which may decrease the effective volume fraction of the ER fluid. For this reason, surface of the titania nanoparticles would be modified with convenient

[a] Gazi University, Chemistry Department, Smart Materials Research Lab., Ankara 06500, Turkey
[b] National Nanotechnology Research Center-UNAM, Bilkent University, Ankara 06800, Turkey

† Footnotes relating to the title and/or authors should appear here.
Electronic Supplementary Information (ESI) available: ATR-FTIR spectra, XPS survey-scan, core-level spectra, TGA curves, ζ-potentials and contact angle images of samples. See DOI: 10.1039/x0xx00000x

molecules or polymers.[25,26] On the other hand, a good ER material should not only show large dielectric constant and proper dielectric loss tangent but also has proper conductivity.[27] Core-shell structured nanocomposites give opportunity to combine dielectric inorganic materials and conducting materials in a unique structure with controlled size, shape and composition. Among the methods to prepare core-shell nanocomposites, modification and functionalization of nanoparticle surfaces are required for the intended applications to enhance the adhesive interactions between inner core and outer shell. In order to obtain functional groups on the surfaces of nanoparticles, a covalent strategy could be exploited to tailor strong and stable binding between the surface of nanoparticles and functional linker groups[28,29] which was also the goal of this current study.

Especially, using conducting polymers as either core or shell species for core-shell structured ER particles have become hot topics.[30] Especially, PEDOT as a derivative of polythiophene has a considerable attention due to its various advantages among the conducting polymers, such as processability in aqueous solution, good thermal and structural stability, low band gap and higher charge carrier mobility due to the electron donating effect of the alkoxy-substituted group.[31] In the literature ER properties of PEDOT and its composites have been reported in limited number of studies. Wang and Jang developed silica/conducting polymer nanospheres[31] and reported that the ER efficiency was correlated with the charge transport behaviour of the conductive polymer shell and PEDOT was slightly more favoured compared to both polypyrrole and polythiophene. In another study, physical adsorption route[32] and Pickering emulsion polymerization[33] was used to fabricate PEDOT/poly(styrene sulfonic acid) coated polystyrene microspheres and PEDOT was used as an electroactive material. Also, PEDOT was used as a conductive filler in poly(dimethylsiloxane)/PEDOT/poly(styrene sulfonic acid)/ ethylene glycol blends as potential actuator materials.[35] None of these PEDOT containing hybrid materials were covalently bonded to their substrates and have focused on the effects of anisotropy on polarizability, dielectric and ER performances of ER dispersions.

In this study, as novel ER materials, core/shell structured nanocomposites that consisted of nanorod and particulate titania cores and conducting polymer PEDOT shells were prepared via bottom-up surface engineering strategy to achieve covalently bonded thin polymer shell and make interfacial interactions between the two components more impressive. The as-obtained nanocomposites were characterized in terms of structural, surface, morphological, thermal, and electrical properties. Antisedimentation stabilities, dielectric properties and ER performances of the core/shell structured TiO_2/PEDOT nanocomposites in SO at various volume fractions were evaluated. The microstructural alterations of the ER fluids under *E* were also revealed by an optical microscope (OM).

Materials and Methods

Materials

Nanoparticle-TiO_2 was kindly supplied by Nanostructured&Amorphous Materials Inc., USA (98% anatase, 15 nm). Silicone oil (SO, η = 1 Pa s, ρ = 0.965 g cm^{-3}) was used for preparing ER fluids and all the other chemicals were Sigma-Aldrich (USA) products with analytical grade and used as received.

Preparation of the samples

Preparation of nanorod-TiO_2. 0.5 g nanoparticle-TiO_2 was dispersed in 10 M $NaOH_{(aq)}$, transferred into a Teflon-lined stainless steel reactor (Berghof BR-200 with BTC-3000 temperature control unit, Germany), and heated at 180°C for 48 h for the hydrothermal treatment. The product was then recovered by centrifugation, washed with deionized water and then treated with 0.1 M $HCl_{(aq)}$ which was then washed with deionized water until the pH was 7. Further, the filtrate was dried under vacuum at 100°C for 24 h.

Surface functionalizations of nanorod-TiO_2. Nanorod-TiO_2 was surface functionalized in two steps to get nucleation points on the particles' surfaces. *(i) surface silanization*: 0.5 g of nanorod-TiO_2 was dispersed in toluene by sonication and 5.85 mL of 3-aminopropyltriethoxysilane (APTS) was added dropwise into the reaction mixture and stirred for 24 h at 70°C. Amino functionalized nanorod-TiO_2 (nanorod-TiO_2-APTS) was obtained with centrifugation, washed with toluene and ethanol, respectively and then dried in a vacuum oven at 75°C for 24 h. *(ii) fabrication of thiophene ended surface*: 0.35 g of nanorod-TiO_2-APTS was dispersed in a reactor in 4-dimethylaminopyridine (DMAP) containing acetonitrile. A freshly prepared solution of 1-(3-dimethylaminopropyl)-3-ethylcarbodiimide hydrochloride (EDAC) and 3-thiophene acetic acid in acetonitrile was added into the above reactor and stirred for 24 h at room temperature. The thiophene ended nanorod-TiO_2 in pale-yellowish colour (nanorod-TiO_2-3TA) was obtained after washing with ethanol and dried under vacuum oven at 65°C for 24 h.

Preparation of covalently bonded nanorod-TiO_2/PEDOT. The nanorod-TiO_2-3TA was dispersed in dodecylbenzene sulfonic acid (DBSA) aqueous solution. 3,4-ethylenedioxythiophene (EDOT) was added into the resultant dispersion and stirred. Then, $FeCl_{3(aq)}$ solution was added into the above reaction mixture by taking the oxidant:monomer molar ratio as 3:2, and stirred under $N_{2(g)}$ atmosphere for 24 h by which the colour of the mixture was changed from white to bluish. The resulting dispersion was washed with deionized water and ethanol, and finally dried in a vacuum oven at 70°C for 24 h.

To make a comparison, the nanoparticle-TiO_2/PEDOT was also synthesized by following the same synthesis procedure described above.

Characterizations

ATR-FTIR spectra of the samples were recorded on Bruker Vertex80 model spectrometer (UK). XPS spectra were recorded on a SPECS XPS spectrometer (Germany) equipped with Mg Kα X-ray source. After peak fitting of the C 1s spectra, all of the spectra were calibrated in reference to the aliphatic C 1s component at a binding energy of 285.0 eV. Powder forms of the samples were used for XRD experiments using a PANalytical MPD X-ray diffractometer (Netherlands) equipped with Cu Kα radiation (λ = 0.51406 nm at 40 mV and 40 mA) at scattering angles from 2° to 80° with a scanning rate of 6° s^{-1}. Morphologies of the samples were investigated with a JEOL JSM 6060 LV model scanning electron microscope (SEM, USA) after coating with gold. For transmission electron microscope (TEM, JEOL JEM-1400 model) measurements, the samples were dispersed in ethanol by sonication and then transferred onto carbon 400 mesh Cu grids by dropping. Thermogravimetric analyses (TGA) of the samples were performed (TA Instruments-Q500, USA) under $N_{2(g)}$ atmosphere with a heating rate of 10°C min^{-1} between 25-700°C. For conductivity and the contact angle measurements, disc shaped pellets were used. The conductivities were determined by four-probe technique (FPP-460A, Entek Elektronik Co., Turkey). The static water contact angle (CA) measurements were conducted at room temperature using a goniometer (CAM 200 Model, KSV, Finland) equipped with a microliter syringe and Olympus Micro DP70 Ver.01.02 camera by recording at least three measurements from three different samples of each material. Deionized water (3 µL, 18 MΩ cm resistivity) was used as the wetting liquid. The densities of the samples were determined with Quantachrome Ultrapycnometer 1000 Model (USA) helium pycnometer at 24°C. The zeta(ζ)-potentials of the colloidal dispersions were measured by a Malvern Nano-ZS ζ-potential analyser (UK) and the pH was adjusted immediately by MPT-2 autotitrator unit at 25°C. Dielectric spectra of the ER fluids (φ =1.25%) were measured at 25°C by an Agilent 4284A model LCR meter (USA) with the measuring cell 16452A model Liquid Test Fixture in a frequency range of 20–10^6 Hz. 1 V of bias electrical potential was applied during the measurements to prevent chain formation in the dispersion.

Antisedimentation stability tests

Antisedimentation stabilities against gravitational forces of the dispersions were determined at 25°C. During the neat eye observations, the height of phase separation between the particle-rich phase and the relatively clear oil-rich phase was recorded as a function of time by using a digital composing stick. The antisedimentation ratio was defined as the height of the particle-rich phase divided to the total height of dispersion.

Microscopic observations

The microstructural changes of the dispersions were investigated under various electric field strengths by an OM equipped with software (OM, LEICA DM LB2, Germany) and the image was captured with LEICA camera. The experimental cell was assembled by mounting two parallel Cu electrodes with approximately 1 mm gap distance on a glass slide, in which a drop of well-mixed ER fluid was dispersed.

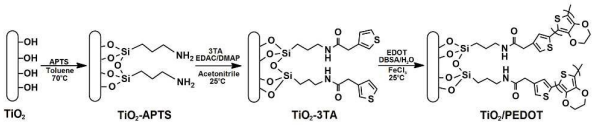

Fig. 1 Schematic representation of the synthesis procedure.

Electrorheological measurements

ER properties of the dispersions (φ =0.625-5%) were measured by a rheometer (Thermo-Haake RS600, Germany) equipped with a high DC voltage generator (HCL 14, FuG Electronik, Germany). The gap between the 35 mm parallel plates was 1.0 mm. All the samples were subjected to pre-shearing (50 s^{-1}) for 60 s and then allowed to equilibrate with the applied electric field (in absence of shear) for 60 s. Three kinds of experiments were then conducted: (*i*) Steady state viscous flow measurements consisted of shear rate ($\dot{\gamma}$) ramps in which shear stress (τ) and viscosity (η) data were collected while the electric field was kept at a different strength for each test, (*ii*) for the dynamic oscillation test, firstly the stress sweep at a constant frequency of 1 Hz was performed to find linear viscoelastic region (LVR), and then the viscoelastic moduli were measured as functions of frequency at constant stresses in the LVR at various electric field strengths (φ = 5%, T = 25°C), (*iii*) for creep-recovery test, a constant stress was applied instantaneously for 100 s to the dispersions under E (τ_0 =30 Pa, φ = 5%, T = 25°C) and change in strains (γ) were measured over a period of time. Then, the stress was removed and the recoverable strains were determined.

Results and Discussion

Characterizations

Covalently bonded, core/shell structured hybrid nanocomposites having rod and particulate geometries were prepared by a multistep process (Figure 1). Confirmations of the surface functionalizations at each step and formations of covalently bonded hybrid nanocomposites were monitored structurally by ATR-FTIR and XPS analyses. ATR-FTIR spectra of bare nanorod-TiO_2, nanorod-TiO_2-APTS, nanorod-TiO_2-3TA, nanorod-TiO_2/PEDOT and PEDOT homopolymer are presented in Figure 2. A broad band between 3600 and 3000 cm^{-1} in the FTIR spectrum indicated the presence of –OH groups on the surface of the nanorod-TiO_2 which enabled to react with coupling agent APTS resulting in amino functionalized surfaces. Additionally, a peak at 1640 cm^{-1} revealed adsorbed water molecules on dried nanorod-TiO_2. After aminosilanization, new bands observed at 2930 and 2864 cm^{-1}, 1479-1316 cm^{-1} and 1636 cm^{-1} were attributed to the C–H stretchings and bendings of methylene groups and N–H stretching vibrations of APTS, respectively. Further bands between 1300 and 1000 cm^{-1} were indications of the Si–O asymmetric vibration stretchings that

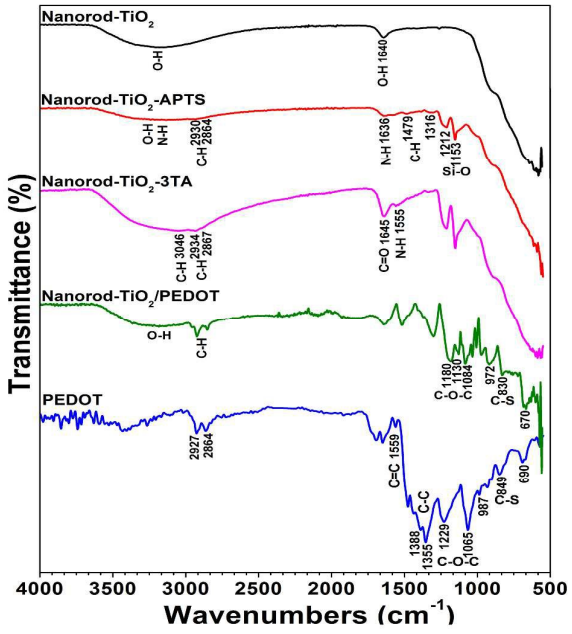

Fig. 2 ATR-FTIR spectra of the samples.

confirmed the presence of ethoxy groups in the APTS condensed with hydroxyl groups on the nanorod-TiO_2 surface resulting in chemically bonded APTS molecules.[35,36] Amide bond formation between 3TA and amino-ended surfaces was supported by the bands appeared at 1645 and 1555 cm^{-1} which were associated with vibration stretchings of C=O and N-H bonds, respectively. The weak band at 3046 cm^{-1} was attributed to the C-H stretchings of the thiophene rings and the peaks at 2934 and 2867 cm^{-1} can be attributed to the asymmetric and symmetric stretchings of the -CH_2- groups.[37] ATR-FTIR spectrum of PEDOT was fully in accordance with the one reported in the literature.[38,39] ATR-FTIR spectrum of nanorod-TiO_2/PEDOT hybrid nanocomposite contained characteristic absorption bands arising from both PEDOT and nanorod-TiO_2. The peaks at 1180, 1130 and 1084 cm^{-1} were attributed to C–O–C bond stretchings. The vibrations at 972, 830 and 670 cm^{-1} were attributed to C–S bond in the thiophene ring; and vibrations at 3000–2800 cm^{-1} were also attributed to the aliphatic C–H stretchings mode due to DBSA molecules.[40] ATR-FTIR spectra of nanoparticle-TiO_2, surface functionalizated-nanoparticle-TiO_2 and nanoparticle-TiO_2/PEDOT can be found in ESI, Figure S1, with similar distinctive characteristic absorptions.

Further evidence of surface functionalizations and PEDOT bonding on the TiO_2 surfaces were provided by XPS analyses. Figure 3 shows the XPS survey-scan spectra of nanorod-TiO_2, nanorod-TiO_2-APTS, nanorod-TiO_2-3TA and nanorod-TiO_2/PEDOT. The survey-scan XPS spectrum of nanorod-TiO_2 showed that bare particles mainly contained Ti, O and C elements. The C 1s peak at binding energy of 285.0 eV was probably due to hydrocarbon contamination of the nanorod-TiO_2 during XPS operation.[41] After modification with APTS, the intensities of the C 1s, Si 2s and Si 2p peaks at 285, 154 and 102 eV, respectively, were increased and N 1s peak was appeared at 399 eV. Apart from these peaks, thiophene ended surfaces showed new signals at about 152 eV and 164 eV which were assigned to S 2s and S 2p, respectively.[37] This result is consistent with a reaction between the –NH_2 group of silane and the –COOH group of 3TA. Similar distinctive characteristic peaks were also observed from XPS survey-scan of nanoparticle-TiO_2, surface modified-nanoparticle-TiO_2 and nanoparticle-TiO_2/PEDOT (ESI, Figure S2).

For further conclusions on the bond formation and molecule configuration on nanorod-TiO_2 surface, core-level XPS spectra of the materials are given in Figure S3 (for C 1s, O 1s, N 1s, Si 2p, S 2p). Before APTS attachment, the C 1s spectrum (curve b in Figure S3) can be fitted into two components with binding energies about 285.0 and 286.8 eV, which were attributed to C-C/C-H and C-O bonds, respectively, probably due to hydrocarbon contamination typically obtained when air exposed samples are introduced into XPS chamber.[41] After APTS grafting, the C 1s spectrum was fitted into two components at 285.0 eV and 286.2 eV which can be attributed to C-C/C-H and C-N bonds, respectively. C 1s fitted spectrum of nanorod-TiO_2-3TA contained peaks corresponding to C-C/C-H (285.0 eV) and C-N/C-S (286.3 eV) bonds beside N-C=O (288.2 eV) bond which were attributed to amide bond formation (curve c in Fig.S3). Exclusive of these peaks, after PEDOT grafting on nanorod-TiO_2 surface intensity of the C 1s signal increased especially due to contribution of DBSA dopant molecules at binding energy of 285.0 eV in addition to the presence of C-O-C and N-C=O bonds at 286.4 and 288.0 eV, respectively (curve d in Figure S3). In the O 1s spectrum (curve b in Figure S3), after APTS grafting, an obvious decrease of the O 1s peak at 529.8 eV (assigned to Ti-O bond) was obtained while a new peak at binding energy of 532.2 eV occurred, which can be attributed to the surface species of O-Si-R.

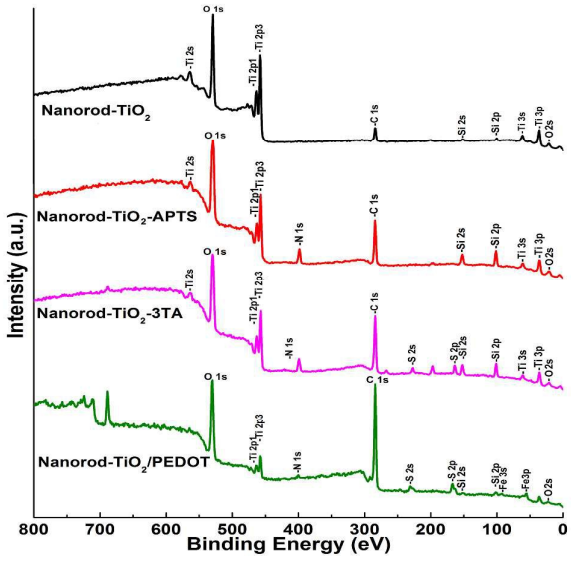

Fig. 3 XPS survey-scan spectra of the nanorod-TiO_2 samples.

The O 1s spectrum for nanorod-TiO_2-3TA was resolved into three components centred at 530.0 eV, 531.5 eV and 532.4 eV, corresponding to O-Ti, O-Si and N-C=O species, respectively (curve c in Figure S3). For nanorod-TiO_2/PEDOT, the intensity of the peak at 530.3 eV, corresponding to O-Ti bond, was decreased due to the thickness of the PEDOT shell. The other two peaks at 531.7 eV and 532.6 eV were also attributed to the $-SO_3^-$ group in DBSA[42] and O-Si and C-O-C bonds in PEDOT.[43] The core-level N 1s spectrum exhibited two clear peaks at 399.2 eV and 400.9 eV after APTS-grafting, which can be assigned to free amine termination (desired silane coupling) and protonated amine (reverse attachment), respectively (curve b in Figure S3). After PEDOT grafting on nanorod-TiO_2 surfaces, the intensity of the N 1s peak at 400.6 eV was decreased and broaden as expected (curve d in Figure S3). APTS-grafting can also be proved by the sharp Si 2p peak at 102.5 eV (curve b in Figure S3) and after PEDOT grafting the intensity of Si 2p peak was obviously decreased due to the thickness of the PEDOT shell on the nanorod-TiO_2 surface (curve d in Figure S3). Nanorod-TiO_2 and nanorod-TiO_2-APTS showed no S 2p signals whereas the high-resolution S 2p spectrum of nanorod-TiO_2-3TA (curve c in Figure S3) consisted the spin-split doublet of S $2p_{3/2}$ and S $2p_{1/2}$ at 164.5 and 165.8 eV, respectively, indicating the presence of C–S bond of thiophene residue.[44] The binding energies of S 2p for nanorod-TiO_2/PEDOT at 163.9 eV/165.2 eV and 168.3 eV/168.7 eV were attributed to the presence of S atoms in thiophene ring in PEDOT and sulfonate in DBSA (curve d in Figure S3), respectively.[45] The signal intensities of N 1s, Ti 2p and Si 2p in the nanorod-TiO_2/PEDOT were reduced and the signal intensities of C 1s, S 2s and S 2p were increased when nanorod-TiO_2 was covered with PEDOT. Additionally, similar results were obtained for nanoparticle-TiO_2 case (ESI, Figure S4). Both FTIR and XPS results indicated that the functionalizations of nanorod and nanoparticle-TiO_2 surfaces and PEDOT graftings onto these surfaces were successfully carried out with bottom-up surface engineering approach.

ζ-potential and water CA measurements also confirmed the surface functionalization and PEDOT grafting on TiO_2 surfaces. The isoelectric point (IEP) obtained from ζ-potential-pH curve of nanorod-TiO_2 was 4.3 which was lower than that of nanoparticle-TiO_2 (IEP=6.1) and attributed to its larger surface area and good adsorption performance[46] (ESI, Figure S5). IEPs of nanorod-TiO_2 and nanoparticle-TiO_2 after APTS functionalizations determined to be 8 and 8.5, respectively, indicating presences of amino-groups on the TiO_2 surfaces.[47] Surface functionalizations of TiO_2-APTS with 3TA decreased the IEPs of both geometries to 7.3 indicating the decrease in the number of amino groups on the particles' surfaces by coupling reaction between amino and carboxylic acid groups. On the other hand, after PEDOT coating of TiO_2-APTS-3TA, the IEPs shifted to 6.6 and 5.7 for nanorod-TiO_2/PEDOT and nanoparticle-TiO_2/PEDOT, respectively.

The contact angle (θ) between the water droplet on the sample and the surface gives information about the ratio between interfacial tensions (water/air, water/solid, and solid/air).[48] For this reason, CA is a useful tool to monitor the alterations on the surfaces of materials. Hydrophilic character of the samples determined to decrease in the following order: nanorod-TiO_2<nanorod-TiO_2-APTS<nanorod-TiO_2-3TA<PEDOT<nanorod-TiO_2/PEDOT and nanoparticle-TiO_2<nanoparticle-TiO_2-APTS<nanoparticle-TiO_2-3TA<PEDOT<nanoparticle-TiO_2/PEDOT (Figure S6). It can be concluded that functionalizations and PEDOT coatings of the both TiO_2 surfaces were successfully performed. Also, water CAs of the both nanocomposites were obtained significantly higher than PEDOT indicating that their hydrophobic characteristics were increased after the grafting processes. It is well known that wettability of solid surface is governed by both the chemical compositions and physical properties of materials. Additionally, surface roughness enhances both the hydrophilicity of hydrophilic surfaces and the hydrophobicity of hydrophobic ones.[49] It can be said that the obtained nanocomposites possessed rougher surfaces with porous loose structures compared to PEDOT.[50]

According to the XRD patterns (Figure 4), nanoparticle-TiO_2 showed peaks at 25.1°, 37.8°, 48.1°, 54.1°, 55.1°, 62.8°, 69.0° and 70.0° which were in good agreement with the anatase phase of TiO_2.[51] These anatase peaks were observed to disappear after alkaline hydrothermal treatment of nanoparticle-TiO_2 for nanorod-TiO_2 fabrication. The peak at 2θ=11.5° was corresponded to 0.77 nm of interlayer spacing between the titanate sheets which can be assigned to the hydrogen titanate structure of nanorod-TiO_2.[52] It was reported that during the nanorod-TiO_2 formation, Ti-O-Ti bonds were broken and replaced with Ti-O-Na bonds to form TiO_6 octahedra frameworks comprised of Na between the interlayers of three dimensional frameworks in highly concentrated $NaOH_{(aq)}$ and at elevated temperatures.[53] After the $HCl_{(aq)}$ treatment, hydrogen-titanate was formed by exchanging Ti-O-Na to Ti-O-H. According to the XRD pattern of PEDOT, a broad peak at 2θ=23.4° was observed which was attributed to the inter-chain planar ring-stacking due to the amorphous nature of the homopolymer.[54,55] For nanorod-TiO_2/PEDOT and nanoparticle-TiO_2/PEDOT nanocomposites, the peaks obtained for nanoparticle-TiO_2 and nanorod-TiO_2 were still observed but became slightly broader after coating with PEDOT.

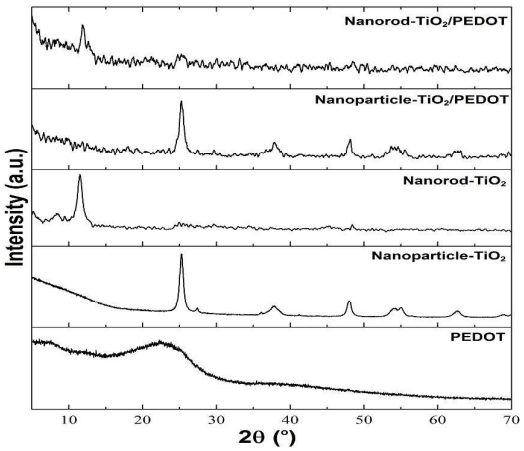

Fig. 4 XRD patterns of the samples.

SEM (Figure 4a) and TEM (Figure 5a) images of the nanoparticle-TiO_2 proved that after alkaline hydrothermal treatment all the nanoparticle-TiO_2 were transformed into rod-like structures (Figures 4b and 5b) with smooth surfaces and with 30-100 nm in diameter and in length of micrometre scale. It is obviously seen that after PEDOT coating, particle size of the nanoparticle-TiO_2/PEDOT was increased due to the core-nanoparticles' tendency to easily form clusters (Figure 5c). On the other hand, it was revealed that uniformly distributed nanorod-TiO_2 particles (Figure 5d) were successfully coated with PEDOT shells with a thickness of 6-7 nm.

Figure 7 shows TGA curves of the materials. The slight weight losses below 110°C were assigned to the physically adsorbed solvent and/or moisture in the samples. PEDOT remained thermally stable up to 300°C and major decomposition occurred between 323-404°C which may be attributed to the decomposition of polymer skeleton; and 48.5% total weight loss was determined at 700°C. For nanorod-TiO_2, continuous degradation occurred until 326°C which was corresponded to the dehydration and the further oxidation with 6.5% total weight loss at 700°C.[56] After surface modification with APTS, continuous weight loss appeared between 240-529°C for nanorod-TiO_2–APTS which was associated with the thermal decomposition of 3-aminopropyl groups and 11% total weight loss occurred at 700°C.[57] On the basis of these results, the grafting ratio of APTS was calculated to be 4.5%. Nanorod-TiO_2-3TA exhibited continuous weight loss between 233-453°C similar with nanorod-TiO_2-APTS and 13% total weight loss was obtained at 700°C thus grafting ratio of 3TA was determined to be 2%. Finally the initial weight loss of ~9% up to ~340°C for nanorod-TiO_2/PEDOT was due to the removal of volatile components, small molecules and dopant anions. Subsequent weight loss between 345-452°C was corresponded to degradation of PEDOT chains and total weight loss was determined to be 32%. Based on the data, the mass ratio of PEDOT in nanorod-TiO_2/PEDOT was estimated to be ~19%. Similar results were determined for nanoparticle-TiO_2, surface functionalized nanoparticle-TiO_2 and nanoparticle-TiO_2/PEDOT (ESI, Figure S7). For nanoparticle-TiO_2, 1.4% weight loss was obtained. Grafting ratios of nanoparticle-TiO_2 were determined as 7.4% and 3.2% after modification with APTS and 3TA, respectively. Grafting ratio of PEDOT was obtained as 17.4% in nanoparticle-TiO_2/PEDOT nanocomposite. According to the TGA results, both nanocomposites had approximately same amount of grafted PEDOT in their structures as targeted.

A summary of the density and conductivity values of the materials are tabulated in Table 1.

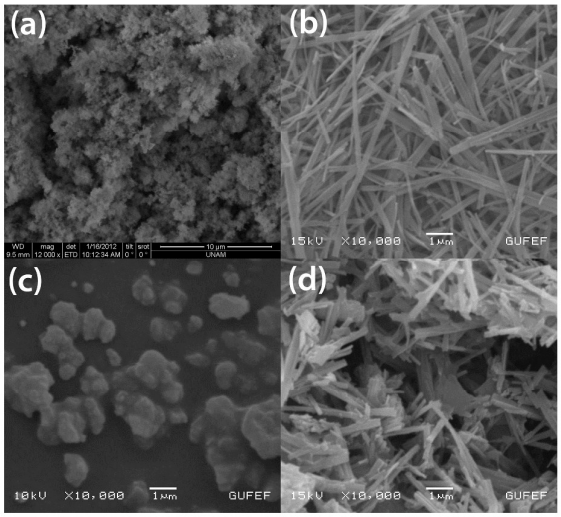

Fig. 5 SEM images of nanoparticle-TiO_2 (a), nanorod-TiO_2 (b), nanoparticle-TiO_2/PEDOT (c) and nanorod-TiO_2/PEDOT (d).

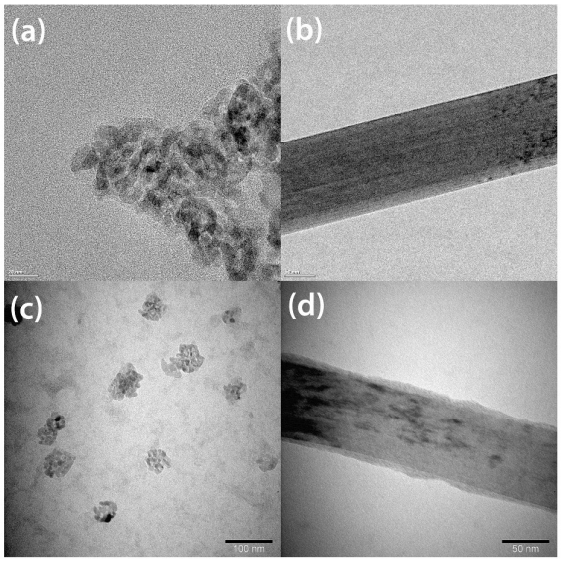

Fig. 6 TEM images of nanoparticle-TiO_2 (a), nanorod-TiO_2 (b), nanoparticle-TiO_2/PEDOT (c) and nanorod-TiO_2/PEDOT (d).

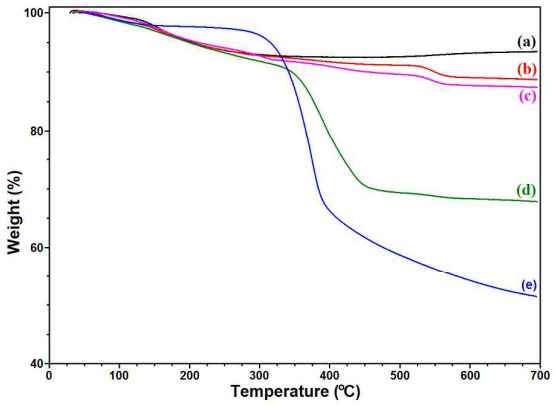

Fig. 7 TGA curves of nanorod-TiO_2 (a), nanorod-TiO_2-APTS (b), nanorod-TiO_2-3TA (c) and nanorod-TiO_2/PEDOT (d) and PEDOT (e).

Table 1 Density and conductivity values of the materials.

Sample	Density (g mL^{-1})	Conductivity (S cm^{-1})	Conductivity after washing with $NH_4OH_{(aq)}$ (S cm^{-1})
Nanoparticle-TiO_2	3.655	$7.5x10^{-7}$	-
Nanorod-TiO_2	3.575	$6.2x10^{-7}$	-
Nanoparticle-TiO_2/PEDOT	2.558	2.63	$6.8x10^{-2}$
Nanorod-TiO_2/PEDOT	2.253	2.69	$7.8x10^{-2}$
PEDOT	1.792	$3.5x10^{2}$	16.4

It was observed that densities of the nanocomposites were lower than core-TiO_2 particles due to coating with low density PEDOT shells as targeted for enhanced colloidal stability. It was also noted that when PEDOT was grafted onto the both TiO_2 particles, higher conductivity values were obtained for the hybrid nanocomposites. Conductivity was originated primarily from the surface coated conducting PEDOT layer. But, these conductivity values were very high for the ER application and to avoid the electrical breakdown under electric field strength, the nanocomposites were further treated with 0.1 M $NH_4OH_{(aq)}$ for overnight for dedoping process[58] and then washed with deionized water until pH≈7. As a result, conductivities of the nanocomposites were reduced ~100X. On the other hand, PEDOT could not be used for ER purposes because of its still high conductivity even though the dedoping process.

Antisedimentation stability

Colloidal stability is one of the important parameters to evaluate whether the ER fluids could find widespread industrial application or not, since the ER activity decreases dramatically along with the sedimentation of dispersed phase. Basically, there are several parameters to influence the colloidal stability of ER dispersions such as type, size, shape and morphology of dispersed particles, type of dispersant medium, particle volume fraction, presence surfactants and density mismatch between dispersed particles and the dispersant. Especially, particle shape and surface properties of the dispersed particles have a greater effect on ER activity and colloidal stability. Particularly, for elongated particles, motions of each particles are restricted due to the entanglement, higher particle-particle interactions due to higher surface area which will lead to improved colloidal stability.[59,60] Sedimentation test at 25°C was used to characterize the dispersion stability of the ER fluids at various volume fractions and their antisedimentation ratios were determined as a function of time. It was observed that antisedimentation ratios of all the ER dispersions were increased with increasing particle volume fractions due to raised particle–particle and particle–fluid interactions (Table 2).[61] It can be said that at higher volume fractions, repulsive forces between dispersed particles and at lower volume fractions, gravitational forces on dispersed particles were dominant. Also, formation of 3D network structures and increased viscosity with increasing particle concentration can be other factors that reduce the rate of sedimentation. At the end of 30 days, there was no phase separation observed for nanorod-TiO_2/PEDOT at volume fraction of 5% as targeted.

Table 2 Antisedimentation ratios of the dispersions at various particle volume fractions at the end of 30 days.

Volume fraction (%)	Antisedimentation ratio (%)			
	Nanoparticle-TiO_2	Nanorod-TiO_2	Nanoparticle-TiO_2/PEDOT	Nanorod-TiO_2/PEDOT
0.625	29	79	20	85
1.25	59	85	21	97
2.5	88	92	35	98
5	91	97	63	100

One-dimensional nano-sized anisotropic rod structure with having high surface area, enhanced rod to rod interactions and creating interparticle entanglements due to their limited rotational motions have led to observe better suspended stability and hindered settling for nanorod-TiO_2/PEDOT. On the other hand, nanoparticle-TiO_2/PEDOT consisted of clusters showed lowest antisedimentation stability against gravitational forces with 63% antisedimentation ratio. It was concluded that particle morphology, size and surface properties are very efficient parameters for the colloidal stability and nanorod-TiO_2/PEDOT/SO system was a perfect candidate for potential industrial applications.

Dielectric properties

Dielectric spectra of the dispersions were recorded using an LCR-meter to further understand their ER responses and the results are given in Figure 8. The Cole–Cole equation (Eqn. 1) was used to fit the dielectric data and to analyse the dielectric characteristics of the dispersions.[62] The lines in the Figure 8 are the fitted results and dielectric parameters of the dispersions obtained from Cole-Cole equation are tabulated in Table 3.

$$\varepsilon^* = \varepsilon' + i\varepsilon'' = \varepsilon_\infty + \frac{\varepsilon_0 - \varepsilon_\infty}{(1+i\omega\lambda)^{1-\alpha}} \quad (0\leq\alpha<1) \qquad (1)$$

In the equation, ε^* is the complex dielectric constant; ε' and ε'' are the dielectric constant and the dielectric loss, respectively; ε_0 and ε_∞ are the static and infinite frequency dielectric constants, ω is angular frequency, λ is dielectric relaxation time denoted by $\lambda = 1/2f_{max}$ (where f_{max} is the relaxation frequency defined by a local maximum of the dielectric loss factor, ε''), α is the scattering degree of relaxation time and $\Delta\varepsilon$ ($\Delta\varepsilon = \varepsilon_0 - \varepsilon_\infty$) shows the difference between the dielectric constant at 0 and infinite frequency. $\Delta\varepsilon$ and λ are related with the magnitude and the rate of the interfacial polarization of the ER fluid, respectively and are considered to be important for observation particle polarizations and strength of the ER fluid.

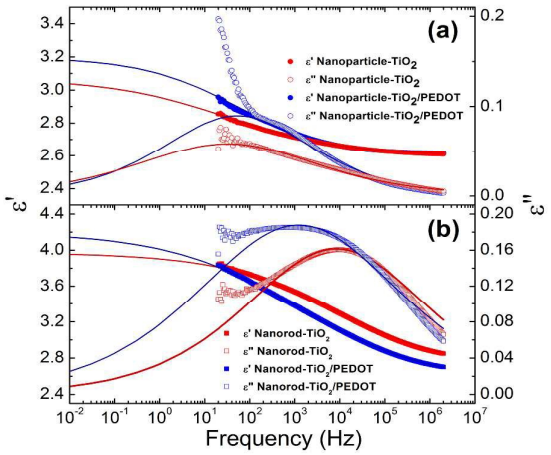

Fig. 8 Dielectric spectra of nanoparticle-TiO_2, nanoparticle-TiO_2/PEDOT (a) and nanorod-TiO_2, nanorod-TiO_2/PEDOT (b) dispersions (Dielectric constant: solid symbol; dielectric loss factor: open symbol, φ =5%).

Table 3 Dielectric parameters of the dispersions obtained from Cole-Cole equation.

Sample (φ=1.25%)	ε_0	ε_∞	$\Delta\varepsilon$	λ (s)	f_{max} (Hz)	α
Nanoparticle-TiO_2	3.07	2.60	0.47	$5x10^{-3}$	32	0.69
Nanoparticle-TiO_2/PEDOT	3.20	2.60	0.60	$3x10^{-3}$	53	0.63
Nanorod-TiO_2	3.97	2.67	1.30	$1.9x10^{-5}$	8377	0.69
Nanorod-TiO_2/PEDOT	4.20	2.52	1.68	$1.3x10^{-4}$	1224	0.72

The proper dielectric loss peak position (f=10^2–10^5 Hz) and large $\Delta\varepsilon$ do not only result in increased interactions between the dispersed particles but also maintain a stable chain structure formed by particles under applied electric and shear fields.[63]

No distinct dielectric loss peak was observed for nanoparticle-TiO_2 and nanoparticle-TiO_2/PEDOT (Figure 8a) whereas, nanorod-TiO_2 and nanorod-TiO_2/PEDOT dispersions gave dielectric loss peaks within 10^2–10^5 Hz (Figure 8b). The achievable polarizability values were obtained as following: $\Delta\varepsilon_{\text{nanorod-TiO2/PEDOT}}>\Delta\varepsilon_{\text{nanorod-TiO2/PEDOT}}>\Delta\varepsilon_{\text{nanoparticle-TiO2/PEDOT}}>\Delta\varepsilon_{\text{nanoparticle-TiO2}}$. It can be concluded that nanorod-TiO_2/PEDOT has stronger interfacial polarization which leads to stiffer chain structures formed by particles under applied E and shows the highest ER activity compared to the particulate nanocomposite. Wang and Zhao reported a relation of ER performance with dielectric characteristics for core/shell kaolinite/TiO_2 particles in which larger dielectric constant enhancement increased the interfacial polarizability of particles and induced higher ER effect.[64] Among the ER fluids examined in this study, nanorod-TiO_2/PEDOT with having the highest $\Delta\varepsilon$ value will lead to possess stronger particle-particle attractions, higher performance in the yield stress and high modulus under E. However, on the basis of relaxation time (λ), core nanorod-TiO_2 might show faster interfacial polarization than that of nanorod-TiO_2/PEDOT under E in terms of dielectric loss model. Therefore, considering both λ and $\Delta\varepsilon$, it can be concluded that the $\Delta\varepsilon$ value is more dominant for ER performance since it is directly related to the strength of fibrillar structures in dispersions.[65] It has been known that high aspect ratio of the dispersed particles plays a dominant role in enhancing the performance of ER fluids.[66] In this study, the geometrical effect originated from aspect ratio and larger magnitude of achieved polarizability gave enhanced ER performance. Furthermore, interfacial polarization was more dominant than conductivity when we considered dielectric properties and conductivity values of the materials.[67]

Optical microscope

The ER fluids were dispersed randomly in SO without applied electric field strength for nanoparticle-TiO_2 (Figure 9a), nanorod-TiO_2 (Figure 9c) and nanoparticle-TiO_2/PEDOT (Figure 9b); and nanorod-TiO_2/PEDOT (Figure 9d) with some aggregations. When electric field was on, the particles started to move parallel to the electric field direction between the electrodes immediately. But it was observed that the microstructural changes under E strongly depended on type of the dispersed phase and particles' volume fraction.

For nanoparticle-TiO_2 and nanoparticle-TiO_2/PEDOT, much denser fibrillar structures were observed after a certain volume fraction. As the volume fractions increased, thicker columnar structures were formed for nanoparticle-TiO_2/PEDOT whereas denser, closer and well aligned fibrillar structures were turned into network structure for nanoparticle-TiO_2. After the network structure formed, the applied electric field did not change its shape and only made the network structure to become much stronger, which was also in good agreement with the ER results. On the other hand, nanorod-TiO_2 and nanorod-TiO_2/PEDOT dispersions formed denser chain structures even for φ=0.0625% and formed network structure at φ = 2.5%. For this reason, φ = 5% was not conducted by OM for rod-like dispersions. Due to their high wetted surface area and rod to rod interactions, one-dimensional structured nanorod-TiO_2 and nanorod-TiO_2/PEDOT particles aligned along the field direction and linked with neighbouring ones with the side by side interactions which led to the formations of more complex structures. According to the previous studies, it was reported that one dimensional elongated particles tend to form complicated dendrite-like network structures under electric field rather than chain-like structures formed by the granular particles.[68-70] Also, this particle overlap can contribute to the solid friction between the neighbouring particles and enhance the yield stress.[13] The electric field induced structures remained stable as long as the electrical field was applied. It was clearly seen that dense fibrillar structures attached at both sides of the electrodes for nanorod-TiO_2/PEDOT which exhibited a higher shear stress compared to nanoparticle-TiO_2/PEDOT dispersion at the same electric field strength.

Electrorheological response: steady state viscous flow

ER properties of the dispersions were studied through a controlled shear rate test under the electric field strength ranging from E = 0.0 to 3.0 kV/mm.

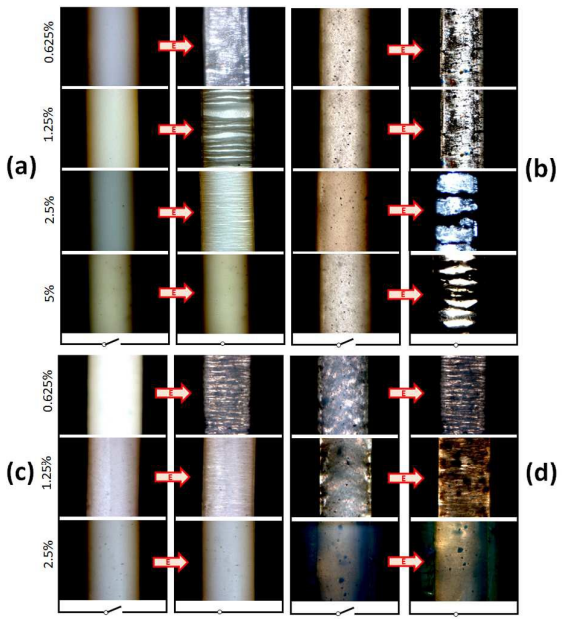

Fig. 9 OM images of nanoparticle-TiO_2 (a), nanoparticle-TiO_2/PEDOT (b), nanorod-TiO_2 (c) and nanorod-TiO_2/PEDOT (d) dispersions at various particle volume fractions.

Figure 10 shows the flow curves of shear stress and shear viscosity as a function of shear rate for the dispersions (φ=5%). In the absence of the electric field, the dispersions showed non-Newtonian shear thinning flow behaviour having low yield stresses even with Newtonian dispersant medium due to the formation of particle network caused by interparticle interactions at high particle volume fractions. The off-field viscosities of the dispersions were about 1.2-1.6 Pa s in the high shear rate region. When the electric field was applied, the viscosities and shear stresses of the dispersions increased abruptly and showed pseudo-plastic behaviours with yield stresses due to the formations of chain-like/columnar or network structures. Also, the shear stresses increased stepwise over the entire shear rate ranges with rising electric field strengths.

The yield stress is one of the critical design parameters for ER fluids. The widely accepted rheological model for ER fluids, i.e. Bingham fluid model, ($\tau = \tau_y + \eta\dot{\gamma}$, where τ is shear stress, τ_y is yield stress, η is viscosity, and $\dot{\gamma}$, is shear rate) could not fit well to the flow curves of our ER systems except nanoparticle-TiO_2, especially in the low shear rate region. This deviation in flow behaviour reflects that the dispersed particles possess a different ER response under electric and shear fields caused by shape and surface chemistry differences of the particles. On the other hand, a suggested equation, the CCJ model, provided more effective fitting for many ER systems[71] and all of the dispersions examined in this study. The CCJ model was applied to describe the flow curves of the dispersions, as shown in Eqn. 2:

$$\tau = \frac{\tau_y}{(1+(t_1\dot{\gamma})^{\alpha})} + \eta_{\infty}(1 + \frac{1}{(t_2\dot{\gamma})^{\beta}})\dot{\gamma} \qquad (2)$$

where α is related to the decline in the stress, t_1 and t_2 are time constants and η_{∞} is the viscosity at a vast shear rate and is interpreted as the viscosity in the absence of an electric field. The exponent β has the range of 0<β≤1, since $d\tau/d\dot{\gamma} \geq 0$ above critical shear rate at which the shear stress becomes a minimum.

In a low shear rate region, the electrostatic interactions induced by electric field strength among the particles were dominant compared to the hydrodynamic interactions induced by the shear flow. The chain-like structures of the particles were started to break down with a further increase in shear rate. The destruction rate of the columnar structures became faster than the reforming rate of columns induced by the electric field above the critical shear rate; thus the flow curves behaved much like those without an electric field. At elevated shear rates, the fibrillar structures were broken into particles or particle clusters by shearing due to the domination of hydrodynamic interactions. For both nanoparticle-TiO_2/PEDOT and nanorod-TiO_2/PEDOT nanocomposite ER systems, the shear stress tended to decline as a function of shear rate to a minimum value and then increased again. The decrease in shear stress at low shear deformations means that reformation of the fibrillar structures was slower than the destruction of field induced fibrillar structures and also reformed structures was not complete similar to those before applying shear deformation.

It was obviously observed that nanorod-TiO_2/PEDOT dispersions had higher critical shear rate and sustained its fibrillar or network structure in a wide range of shear deformations. Interestingly, although the surface properties were similar for the both nanocomposites, the ER effect increased after nanorod-TiO_2 was coated with PEDOT layers with fine distributions, whereas decreased after nanoparticle-TiO_2 was coated with PEDOT with clusters. It could be attributed to their final structures compared with their uncoated core nanoparticles.

The τ_y values determined according to CCJ model and their dependence on φ and E are given in Figure 11. It was observed that τ_y was increased with increasing φ and E which suggested that the particle-particle interactions and electrostatic forces became strong enough to resist against the hydrodynamic forces.

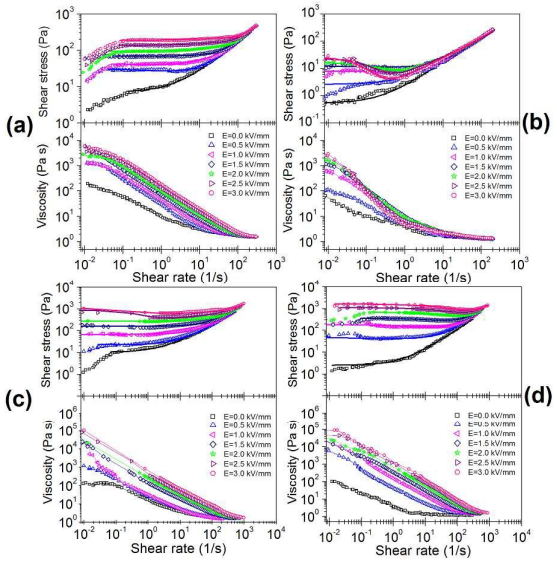

Fig. 10 Flow curves of nanoparticle-TiO_2 (a), nanoparticle-TiO_2/PEDOT (b) nanorod-TiO_2 (c) and nanorod-TiO_2/PEDOT (d) dispersions (Solid lines in shear stress-shear rate curve were fitted using the suggested CCJ model, φ = 5%.

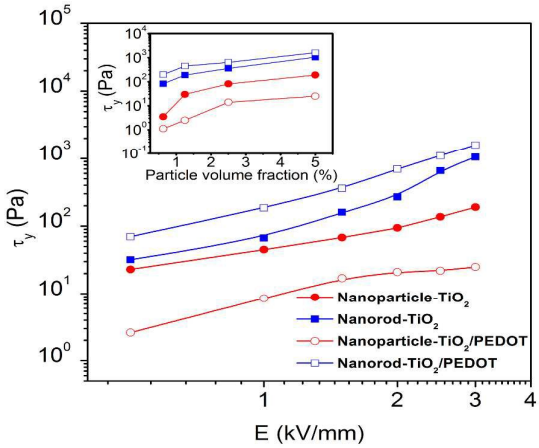

Fig. 11 Change in the τ_y values determined according to CCJ model with φ and E.

Dynamic oscillatory

Small amplitude dynamic oscillatory test is an effective method to investigate viscoelastic phenomena related to the existence of solid-like structures which allows one to determine the particle-particle interactions while minimizing the influence of the external flow deformations.[72] The linear viscoelastic region (LVR), where deformations are so small to produce changes in the structure of a material and moduli do not depend on deformation, was first determined via amplitude sweep at a fixed frequency of 1 Hz as a function of *E*. Then frequency sweep was carried out in the predetermined LVR. Without electric field, the storage (G′) moduli were constant only up to very low shear stress values. The maximum applicable shear stresses were observed as following (E = 3 kV/mm φ = 5%): $\tau_{nanorod\text{-}TiO2/PEDOT}$ = 640 Pa>$\tau_{nanorod\text{-}TiO2}$ = 160 Pa>$\tau_{nanoparticle\text{-}TiO2}$ = 40 Pa>$\tau_{nanoparticle\text{-}TiO2/PEDOT}$ = 15 Pa. The maximum applicable shear stress can be identified beyond which the G′ ceases to be constant and decreases rapidly with increasing shear stress.

Figure 12 shows the frequency dependence of storage (G′) and loss (G″) moduli for various electric field strengths for the dispersions. The results agree with those of steady state rheological measurements. Without an electric field, G″ was smaller than the G′ for nanoparticle-TiO_2 and nanorod-TiO_2 dispersions and showed an increase with rising frequency. This indicated that weak 3D structure formations resulted in elastic interactions which may be attributed to the higher particle volume fraction and larger probability of particle-particle interactions. But for the nanocomposites, G′ and G″ values were closer to each other and increased with increasing frequency hence, G″ became dominant at higher frequencies indicating viscous-like structures without *E*.

With applied *E*, G′ values significantly increased and began to dominate over G″ values and stable plateau regions were observed in a wide frequency range indicating that the dispersions showed solid-like elastic behaviour. These increments were significant for nanorod-TiO_2/PEDOT dispersions compared to the particulate one. It can be said that rod-like structure will be more suitable for vibration damping applications. Compared to others, the nanorod-TiO_2/PEDOT dispersion possessed higher storage moduli. At constant conditions (f=1 Hz and E=3 kV mm^{-1}) the G′ values of the dispersions were determined as following: $G'_{nanorod\text{-}TiO2/PEDOT}$ = 206 MPa>$G'_{nanorod\text{-}TiO2}$ = 170 MPa>$G'_{nanoparticle\text{-}TiO2}$ = 37 MPa>$G'_{nanoparticle\text{-}TiO2/PEDOT}$ = 10.5 MPa. This revealed that the nanorod-TiO_2/PEDOT showed higher rigidity under electric fields, which is also in accordance with its higher yield stress. Therefore, both steady shear viscosity and dynamic viscoelastic results indicate that the nanorod-TiO_2/PEDOT dispersion exhibited enhanced ER effect compared to the nanorod-TiO_2 and nanoparticle-TiO_2/PEDOT dispersions. The ER enhancement may be attributed to several reasons including increased polarizability, interparticle friction and viscous drag force that stem from elongated structure and increased colloidal stability.[73]

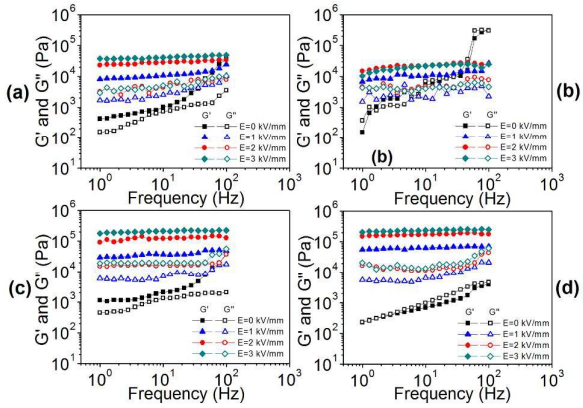

Fig. 12 Frequency dependence of G′ and G″ for various electric field strengths for the dispersions (G′: full symbols, G″: open symbols, φ = 5%, f = 1 Hz).

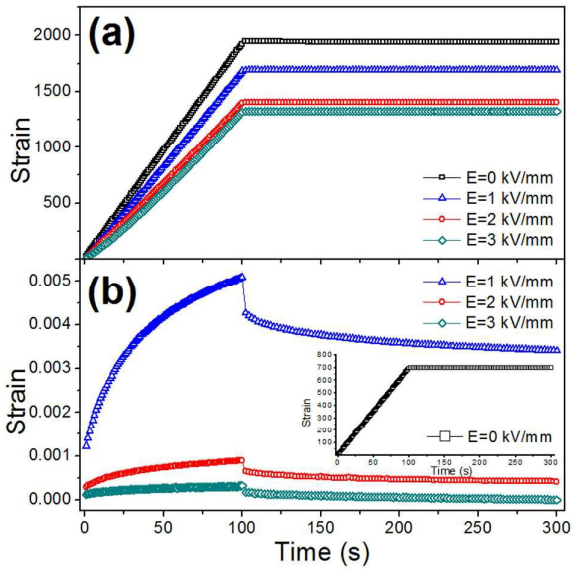

Fig. 13 Change in strain with time at various electric field strengths under creep-recovery test for nanoparticle-TiO_2/PEDOT (a) and nanorod-TiO_2/PEDOT (b) (τ_0 = 30 Pa for the first 100 s and then τ_0 = 0 Pa, φ = 5%,).

Creep and creep-recovery

Creep and creep-recovery tests are beneficial experiments to understand the mechanism behind the rheological properties and time dependent mechanical behaviour of the materials.[74] For nanoparticle-TiO_2/PEDOT dispersion (Figure 13a) under all the electric field strengths and for nanorod-TiO_2/PEDOT dispersion (Figure 13b) under no electric field strength, strain values were increased linearly under applied stress with time and after removing the applied stress no recovery took place. It means that they behaved like viscous materials under those conditions. This applied stress value was higher than the yield stresses of nanoparticle/PEDOT dispersion under all the *E* cases. For this reason, the results were in accordance with steady state flow measurements.

On the other hand, nanorod-TiO_2/PEDOT dispersion represented time-dependent non-linear viscoelastic deformation under applied stress and subsequent time-dependent reformation after setting the applied stress to $\tau = 0$ Pa. Instantaneous decrease in strain corresponded to the elastic recovery and subsequent reversible viscoelastic recoveries were obtained under *E* in the recovery process. This viscoelastic response of the nanorod-TiO_2/PEDOT dispersion arose from the fibrillar aggregates of the dispersed particles which was indication of solid-like behaviour under *E*. For the case of nanoparticle-TiO_2/PEDOT, above the yield point, the fibrillar structures were repeatedly broken down and could not reform which resulted with viscous flow. The strain values obtained in creep-recovery process were decreased with increasing *E* indicating that nanorod-TiO_2/PEDOT dispersion formed stronger solid-like structure.

The recovery ratio (χ) is defined to evaluate the elasticity of the ER fluid and calculated from the following equation,[75]

$$\chi = \frac{\gamma_i - \gamma_f}{\gamma_i} \quad (3)$$

where γ_i is the total strain acquired before removing the applied stress and γ_f is the average steady state strain after removal of the applied stress. For nanorod-TiO_2/PEDOT dispersion, recovery ratios with increasing *E* were calculated as following: $\chi_{E=1\ kV/mm}=0.33<\chi_{E=2\ kV/mm}=0.54<\chi_{E=3kV/mm}=0.98$. It was concluded that in the recovery phase, the deformation of the nanorod-TiO_2/PEDOT dispersion could be recovered almost completely under higher electric fields indicating enhanced elastic interaction of the dispersed particles.

Conclusions

Nanorod-TiO_2 core were synthesized via alkaline-hydrothermal process. Surface functionalizations with bottom-up approach and PEDOT formation on the surfaces of particulate and rod-like TiO_2 were proven by ATR-FTIR, XPS, TEM, ζ-potential and CA measurements. Colloidal stability was improved by preparing polymer coated nanorod structures showing no sedimentation at $\varphi = 5\%$. Consequently, higher wetted surface area and rod-to-rod interactions besides larger achievable polarizability and short relaxation time of interfacial polarization made synergistic effect and with the help of enhanced colloidal stability, core/shell structured nanorod-TiO_2/PEDOT particles showed stronger ER activity and storage modulus besides higher creep-recovery after stress loading compared to the particulate case.

Acknowledgements

The authors are grateful to the European Science Foundation through COST CM1101 Action, the Turkish Scientific and Technological Research Council (TUBITAK) for the financial support of this work (Grant No: 111T637) and for the PhD scholarship provided to O.E. (TUBITAK-BIDEB). The authors thank to Z. Suludere for TEM measurements and F. Unal for OM measurements.

Notes and references

1 T. Hao, *Adv. Mater.*, 2001, **13**, 1847.
2 J. Madeja, Z. Kesy and A. Kesy, *Smart Mater. Struct.*, 2011, **20**, 105005.
3 N. Wereley, J. Lindler, N. Rosenfeld and Y.-T. Choi, *Smart Mater. Struct.*, 2004, **13**, 743.
4 Q-H. Nguyen and S-B. Choi, *Smart Mater. Struct.*, 2009, **18**, 115020.
5 K. Bohon and S. Krause, *J. Polym. Sci. Pol. Phys.*, 1998, **36**, 1091.
6 Y. Y. Tsai, C.H. Tseng and C. K. Chang, *J. Mater. Process. Tech.*, 2008, **201**, 565.
7 P. Sheng and W. Wen, *Annu. Rev. Fluid Mech.*, 2012, **44**, 143.
8 J. Yin and X. Zhao, *Colloid. Surface. A*, 2008, **329**, 153.
9 M. M. Ramos-Tejada, M. J. Espin, R. Perea and A. V. Delgado, *J. Non-Newton. Fluid*, 2009, **159**, 34.
10 B. Sim and H. J. Choi, *RSC Adv*, 2015, **5**, 11905.
11 J. Yin, X. Xia, L. Xiang, Y. Qiao and X. Zhao, *Smart Mater. Struct.*, 2009, **18**, 095007.
12 M. Sedlacik, M. Mrlik, Z. Kozakova, V. Pavlinek and I. Kuritka, *Colloid Polym. Sci.*, 2013, **291**, 1105.
13 J. Wu, T. Jin, F. Liu, J. Guo, P. Cui, Y. Cheng and G. Xu, *J. Mater. Chem. C*, 2014, **2**, 5629.
14 S. Y. Oh and T. J. Kang, *Soft Matter*, 2014, **10**, 3726.
15 J. Yin, X. Zhao, L. Xiang, X. Xia and Z. Zhang, *Soft Matter*, 2009, **5**, 4687.
16 J. A. Marins, B. G. Soares, A. A. Silva and S. Livi, *RSC Adv.*, 2014, **4**, 50925.
17 H. J. Choi, M. S Choa, K-K. Kang and W-S. Ahn, *Micropor. Mesopor. Mat.*, 2000, **39**, 19.
18 Y. Tian, Y. Meng and S. Wen, *Mater. Lett.*, 2001, **50**, 120.
19 O. Erol, H. I. Unal and B. Sari, *Polym. Composite.*, 2010, **31**, 471.
20 Y. D. Liu, F. F. Fang, H. J. Choi and Y. Seo, *Colloid. Surface. A*, 2011, **381**, 17.
21 J. Yin, X. Xia, L. Xiang and X. Zhao, *Carbon*, 2010, **48**, 2958.
22 H. Y. Kim and H. J. Choi, *RSC Adv.*, 2014, **4**, 28511.
23 K. Tanaka, T. Wakayasu, A. Kubono and R. Akiyama, *Sensor. Actuat. A-Phys.*, 2004, **112**, 376.
24 J. Yin, Y. Shui, Y. Dong and X. Zhao, *Nanotechnology*, 2014, **25**, 045702.
25 Y. D. Liu, F. F. Fang and H. J. Choi, *Mater. Lett.*, 2010, **64**, 154.
26 J. Yin, X. Xia, L. Xiang and X. Zhao, *J. Mater. Chem.*, 2010, **20**, 7096.
27 J. Wu, G. Xu, Y. Cheng, F. Liu, J. Guo and P. Cui, *J. Colloid Interf. Sci.*, 2012, **378**, 36.
28 N. Esman, A. Peled, R. Ben-Ishay, Y. Kapp-Barnea, I. Grigoriants and J-P. Lellouche, *J. Mater. Chem.*, 2012, **22**, 2208.
29 I. K. Herrmann, R. N. Grass, D. Mazunin and W. J. Stark, *Chem. Mater.*, 2009, **21**, 3275.
30 Y. D. Liu and H. J. Choi, *Soft Matter*, 2012, **8**, 11961.
31 J-Y. Hong and J. Jang, *Soft Matter*, 2010, **6**, 4669.
32 Y. D. Liu, J. E. Kim and H. J. Choi, *Macromol. Rapid Comm.*, 2011, **32**, 881.
33 S. H. Kim, J. H. Kim, H. J. Choi and J. Park, *RSC Adv.*, 2015, **5**, 72387.
34 W. Wichiansee and A. Sirivat, *Mater. Sci. Eng. C*, 2009, **29**, 78.
35 M. Sabzi, S. M. Mirabedini, J. Zohuriaan-Mehr and M. Atai, *Prog. Org. Coat.*, 2009, **65**, 222.
36 G. Wang, G. Chen, Z. Wei, T. Yu, L. Liu, P. Wang, Y. Chang and M. Qi, *J. Appl. Polym. Sci.*, 2012, **125**, 3871.

37 M.-D. Lu and S.-M. Yang, *J. Colloid Interf. Sci*., 2009, **333**, 128.
38 J. W. Choi, M. G. Han, S. Y. Kim, S. G. Oh and S. S. Im, *Synthetic Met*., 2004, **141**, 293.
39 Y. Wen, J. Xu, H. He, B. Lu, Y. Li and B. Dong, *J. Electroanal. Chem*., 2009, **634**, 49.
40 S. Sarmah and A. Kumar, *Phys. Status Solidi A*, 2012, **209**, 2546.
41 Y.-Y. Song, H. Hildebrand and P. Schmuki, *Surf. Sci*., 2010, **604**, 346.
42 W. Prissanaroon, N. Brack, P.J. Pigramand and J. Liesegang, *Surf. Interface Anal*., 2003, **35**, 974.
43 A. Lisowska-Oleksiak, A. P. Nowak, M. Wilamowska, M. Sikora, W. Szczerba and C. Kaputsa, *Synthetic Met*., 2010, **160**, 1234.
44 G. Greczynski, T. Kugler and W. R. Salaneck, *Thin Solid Films*, 1999, **354**, 129.
45 E. Montibon, L. Jarnstrom and M. Lestelius, *Cellulose*, 2009, **16**, 807.
46 W. Liu, W. Sun, A. G. L. Borthwick and J. Ni, *Colloid. Surface. A,* 2013, **434**, 319.
47 E. Ukaji, T. Furusawa, M. Sato and N. Suzuki, *Appl. Surf. Sci*., 2007, **254**, 563.
48 C. Wang, H. Mao, C. Wang and S. Fu, *Ind. Eng. Chem. Res*., 2011, **50**, 11930.
49 L. Xu, W. Chen, A. Mulchandani and Y. Yan*, Angew. Chem. Int. Edit*., 2005, **44**, 6009.
50 W. Zhong, S. Liu, X. Chen, Y. Wang and W. Yang, *Macromolecules,* 2006, **39**, 3224.
51 X. Lu, Q. Zhao, X. Liu, D. Wang, W. Zhang, C. Wang and Y. Wei, *Macromol. Rapid Comm*., 2006, **27**, 430.
52 K. Kiatkittipong, J. Scott and R. Amal, *ACS Appl. Mater. Inter*., 2011, **3**, 3988.
53 T. Kasuga, *Thin Solid Films,* 2006, **496**, 141.
54 Y-K Han, J-N Yih, M-Y Chang, W-Y Huang, K-S Ho, T-H Hsieh and J-G Lou, *Macromol. Chem. Physic.*, 2011, **212**, 361.
55 S. V. Selvaganesh, J. Mathiyarasu, K.L.N. Phani and V. Yegnaraman, *Nanoscale Res. Lett.,* 2007, **2**, 546.
56 J.-C. Xu, M. Lu, X-Y. Guo and H-L. Li, *J. Mol. Catal. A-Chem*., 2005, **226**, 123.
57 M. Z. Kassaee, H. Masrouri and F. Movahedi, *Appl. Catal. A-Gen*., 2011, **395**, 28.
58 T-C. Tsai, H-C. Chang, C-H. Chen, Y-C. Huang and W-T. Whang, *Org. Electron*., 2014, **15**, 641.
59 B. Wang and X. Zhao, *Adv. Funct. Mater,* 2005, **15**, 1815.
60 R. V. Upadhyay, Z. Laherisheth and K. Shah, *Smart Mater. Struct*., 2014, **23**, 015002.
61 G. T. Ngatu, N. M. Wereley, J. O. Karli and R. C. Bell, *Smart Mater. Struct*., 2008, **17**, 045022.
62 K. S. Cole and R. H. Cole, *J. Chem. Phys*. 1941, **90**, 341.
63 Q. Cheng, V. Pavlinek, Y. He, C. Li and P. Saha, *Colloid Polym. Sci*., 2009, **287**, 435.
64 B. Wang and X. Zhao, *Langmuir,* 2005, **21**, 553.
65 M. S. Cho, H. J. Choi and W-S. Ahn, *Langmuir,* 2004, **20**, 202.
66 J-Y. Hong, M. Choi, C. Kim and J. Jang, *J. Colloid Interf. Sci*., 2010, **347**, 177.
67 F. Ikazaki, A. Kawai, K. Uchida, T. Kawakami, K. Edamura, K. Sakurai, H. Anzai and Y. Asako, *J. Phys. D: Appl. Phys*., 1998, **31**, 336.
68 J. Yin, X. Zhao, X. Xia, L. Xiang and Y. Qiao, *Polymer,* 2008, **49**, 4413.
69 M. T. López-López, P. Kuzhir, G. Bossis, *J. Rheol*. 2009, **53**, 115.
70 R.C. Bell, J.O. Karli, A.N. Vavreck, D.T. Zimmerman, G.T. Ngatu and N.M. Wereley, *Smart Mater. Struct*., 2008, **17**, 015028.
71 M.S. Cho, H.J. Choi and M.S. Jhon, *Polymer,* 2005, **46**, 11484.
72 O. Erol, M. M. Ramos-Tejada, H. I. Unal and A. V. Delgado, *J. Colloid Interf. Sci*., 2013, **392**, 75.
73 J. Yin, X. Wang, R. Chang and X. Zhao, *Soft Matter*, 2012, **8**, 294.
74 Y. Xu, X. Gong, S. Xuan, X. Li, L. Qin and W. Jiang, *Soft Matter,* 2012, **8**, 8483.
75 Y.D. Liu, X. Quan, B. Hwang, Y.K. Kwon and H.J. Choi, *Langmuir,* 2014, **30**, 1729.

RSC Advances

ARTICLE

Graphical abstract

Covalently-bonded core/shell structured nanorod-TiO_2/PEDOT nanocomposite is fabricated successfully and electric field response is compared with particulate one. Higher wetted surface area, rod-to-rod interactions and conducting thin shell make synergistic effect on polarizability under electric field and colloidal stability against sedimentation and this induces nanorod-TiO_2/PEDOT to show stronger ER activity, storage modulus and higher creep-recovery after stress loading compared to nanoparticle-TiO_2/PEDOT.